Title

Additional chain-branching pathways in the low-temperature oxidation of branched alkanes

Authors

Wang, Zhandong
Zhang, Lidong
Moshammer, Kai
et al.

Publication Date

2016-02-01

DOI

10.1016/j.combustflame.2015.11.035

Peer reviewed

Combustion and Flame 164 (2016) 386–396

Contents lists available at ScienceDirect

Combustion and Flame

journal homepage: www.elsevier.com/locate/combustflame

Additional chain-branching pathways in the low-temperature oxidation of branched alkanes

Zhandong Wang[a,*], Lidong Zhang[b], Kai Moshammer[c], Denisia M. Popolan-Vaida[d,e], Vijai Shankar Bhavani Shankar[a], Arnas Lucassen[f], Christian Hemken[g], Craig A. Taatjes[c], Stephen R. Leone[d,e], Katharina Kohse-Höinghaus[g], Nils Hansen[c], Philippe Dagaut[h], S. Mani Sarathy[a,*]

[a] Clean Combustion Research Center, King Abdullah University of Science and Technology, Thuwal 23955-6900, Saudi Arabia
[b] National Synchrotron Radiation Laboratory, University of Science and Technology of China, Hefei, Anhui 230029, PR China
[c] Combustion Research Facility, Sandia National Laboratories, Livermore, CA 94551, USA
[d] Departments of Chemistry and Physics, University of California, Berkeley, CA 94720, USA
[e] Chemical Sciences Division, Lawrence Berkeley National Laboratory, Berkeley, CA 94720, USA
[f] Physikalisch-Technische Bundesanstalt, Bundesallee 100, D-38116 Braunschweig, Germany
[g] Department of Chemistry, Bielefeld University, D-33615 Bielefeld, Germany
[h] Centre National de la Recherche Scientifique (CNRS), INSIS, 1C, Avenue de la recherche scientifique, 45071, Orléans Cedex 2, France

ARTICLE INFO

Article history:
Received 11 September 2015
Revised 4 November 2015
Accepted 6 November 2015
Available online 31 December 2015

Keywords:
Auto-oxidation
Chain-branching
Highly oxidized multifunctional molecules
Peroxides
Alternative isomerization
Synchrotron VUV photoionization mass spectrometry

ABSTRACT

Chain-branching reactions represent a general motif in chemistry, encountered in atmospheric chemistry, combustion, polymerization, and photochemistry; the nature and amount of radicals generated by chain-branching are decisive for the reaction progress, its energy signature, and the time towards its completion. In this study, experimental evidence for two new types of chain-branching reactions is presented, based upon detection of highly oxidized multifunctional molecules (HOM) formed during the gas-phase low-temperature oxidation of a branched alkane under conditions relevant to combustion. The oxidation of 2,5-dimethylhexane (DMH) in a jet-stirred reactor (JSR) was studied using synchrotron vacuum ultraviolet photoionization molecular beam mass spectrometry (SVUV-PI-MBMS). Specifically, species with four and five oxygen atoms were probed, having molecular formulas of $C_8H_{14}O_4$ (e.g., diketo-hydroperoxide/keto-hydroperoxy cyclic ether) and $C_8H_{16}O_5$ (e.g., keto-dihydroperoxide/dihydroperoxy cyclic ether), respectively. The formation of $C_8H_{16}O_5$ species involves alternative isomerization of OOQOOH radicals via intramolecular H-atom migration, followed by third O_2 addition, intramolecular isomerization, and OH release; $C_8H_{14}O_4$ species are proposed to result from subsequent reactions of $C_8H_{16}O_5$ species. The mechanistic pathways involving these species are related to those proposed as a source of low-volatility highly oxygenated species in Earth's troposphere. At the higher temperatures relevant to auto-ignition, they can result in a net increase of hydroxyl radical production, so these are additional radical chain-branching pathways for ignition. The results presented herein extend the conceptual basis of reaction mechanisms used to predict the reaction behavior of ignition, and have implications on atmospheric gas-phase chemistry and the oxidative stability of organic substances.

1. Introduction

The low-temperature auto-oxidation of hydrocarbons occurs in many natural and engineered systems. Gas-phase auto-oxidation determines the fate of volatile organic compounds (VOCs) in the atmosphere under low-NO_x conditions [1–4], ultimately leading to the formation of extremely low volatility organic compounds (ELVOCs) [1,5,6]. In combustion systems, low-temperature auto-oxidation of hydrocarbon fuel leads to ignition [7–13], a governing parameter in the design of engines. In the liquid phase, auto-oxidation contributes to the degradation of organic substances such as lipids, lubricants, plastics, and foods [14–20]. Simulations attempting to predict the ignition properties of a hydrocarbon fuel in engines or the distribution of atmospheric pollutants must accurately represent the complex auto-oxidation pathways and branching ratios to various products [21–24].

* Corresponding author.
E-mail addresses: zhandong.wang@kaust.edu.sa (Z. Wang), mani.sarathy@kaust.edu.sa (S.M. Sarathy).

http://dx.doi.org/10.1016/j.combustflame.2015.11.035
0010-2180/

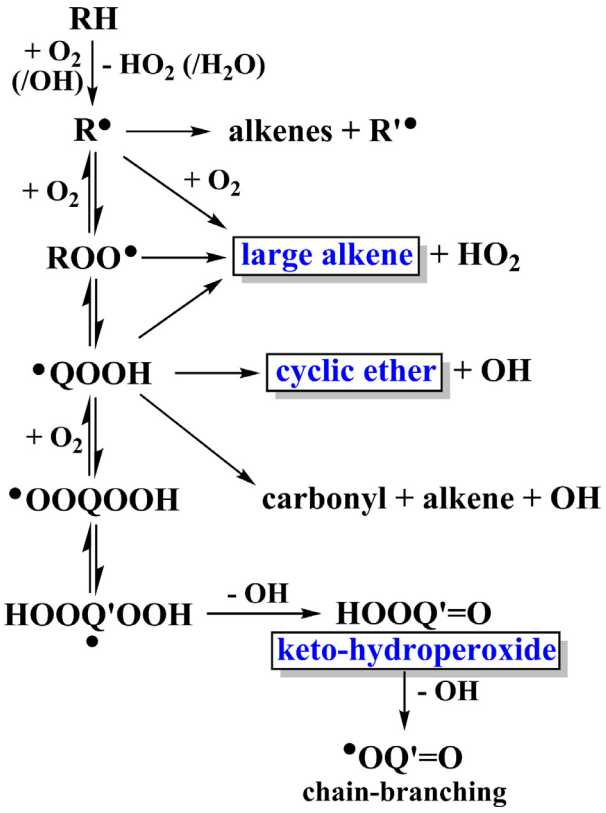

Scheme 1. Classical scheme for the low-temperature oxidation of hydrocarbons. The annotated species with blue and box were detected in this work. (For interpretation of the references to color in this figure legend, the reader is referred to the web version of this article.)

The auto-oxidation process begins with radical initiation and proceeds by a series of O_2 addition and intramolecular H-atom migration reactions that eventually lead to radical chain-branching, propagation, or termination [7–12], as presented in Scheme 1 (see Supporting Information, SI, for detailed description). This scheme dating back to the mid 20th century [7,8] laid the foundation for the first mathematical models for predicting ignition [13,25]. At present, the scheme remains largely unchanged in high fidelity chemical kinetic simulations used to improve the efficiency and emissions of combustion systems [11,26–29].

The classical low-temperature auto-oxidation reaction scheme presented in Scheme 1 has been confirmed via gas-phase measurements of the key intermediates such as hydroperoxyalkyl radicals [30], alkylhydroperoxides [31,32], large alkenes [32–35], cyclic ethers [31,34,36,37], and keto-hydroperoxides [33,35,38–42]. Experiments on liquid-phase auto-oxidation by Korcek and coworkers [43–46] identified the presence of monohydroperoxides, dihydroperoxides, and keto-hydroperoxides, while recent computational studies [47,48] have shown that subsequent decomposition pathways of keto-hydroperoxides to acids are favorable. The recent experimental study on dimethyl ether oxidation [42] confirms this mechanism, i.e., the formation of carbonic acid.

The majority of studies on low-temperature hydrocarbon auto-oxidation use propane [37] or *n*-butane [32], as these prototypical *n*-alkanes display the cool-flame and negative temperature coefficient (NTC) characteristics observed in larger alkanes. *n*-Heptane and *iso*-octane are also commonly used surrogate compounds to understand the ignition chemistry of real gasoline fuels [23,24].

In this work, we used a jet-stirred reactor (JSR) to investigate the auto-oxidation of 2,5-dimethylhexane (DMH), a lightly methyl substituted alkane that is in the typical carbon number range of gasoline fuel. This molecule was chosen because the presence of primary, secondary, and tertiary carbon hydrogen bonds was expected to yield more complexity in the low-temperature reaction scheme (as discussed later). Furthermore, DMH is a model compound to study the combustion properties of lightly branched alkanes, which are major components of typical petroleum derived and synthetic fuels [49,50].

Product species measured in our experiments provide further confirmation of the classical low-temperature oxidation scheme. However, we also observe more highly oxygenated species that are not part of the classical scheme. A detailed kinetic analysis was conducted to rationalize formation pathways leading to these species. We show that these new species are additional radical chain-branching intermediates, suggesting the presence of an extended auto-oxidation reaction mechanism for DMH at conditions of relevance to auto-ignition in engines. Our experimental evidence of an extended auto-oxidation scheme also has implications on atmospheric gas-phase chemistry and on the oxidative stability of liquid hydrocarbons.

2. Experimental and theoretical method

In this study, a spherical fused-silica JSR was coupled to a high resolution ($m/\Delta m \sim 2500$) time-of-flight molecular-beam mass spectrometer (MBMS, refers to Fig. S1 in SI) with synchrotron vacuum ultraviolet (SVUV) radiation as the photoionization (PI) source [42]. The mass spectrometer has a sensitivity range of 1 ppm, and a dynamic range of several orders of magnitude. The SI presents detailed information on the experimental method and a diagram of the set-up in Fig. S1. The experiments were performed at Terminal 3 of the Chemical Dynamics Beamline of the Advanced Light Source at the Lawrence Berkeley National Laboratory, USA. The SVUV-PI-MBMS enables detection of reactive oxidation intermediates, e.g., peroxides [31,42,51]. The stoichiometric DMH (1%)/O_2/Ar mixtures were investigated under quasi-atmospheric pressures and residence times of 0.933 bar and 2 s, respectively. A K-type thermocouple from Thermocoax was fixed at the vicinity of the sampling cone to measure the reactor temperature. The thermocouple is coated with Inconel alloy 600, which is not expected to catalyze the oxidation reaction under the conditions studied here. Experiments conducted without the thermocouple in place detected similar species distributions in the reactor. The uncertainty in reactor temperature is ±20 K, which was obtained by measuring the temperature distribution inside the JSR with a movable thermocouple. The photoionization spectra were measured at varying reactor temperatures to obtain the distribution of reactive intermediates. Furthermore, photoionization efficiency spectra (PIE) were measured to obtain species' ionization thresholds to aid identification [52]. Absolute mole fractions are not presented due to the absence of photoionization cross sections for many of the detected species.

The mass resolution and the resolution of photoionization spectroscopy for species this large preclude the unambiguous identification of the observed molecules simply by a combination of mass and photoionization spectra. However, we can limit the conceivable range of chemical pathways based on the knowledge of global hydrocarbon oxidation chemistry; for example, no significant molecular weight growth by carbon–carbon bond formation occurs at these stoichiometries and temperatures. The present approach is to combine existing knowledge on low-temperature oxidation mechanisms, chemical kinetics, and theoretical calculations to support the interpretation of experimental data.

The identification of species at certain mass-to-charge (m/z) signals is performed by first postulating potential structures based on the classical low-temperature reaction scheme. For m/z signals that cannot be explained by the classical scheme, the mechanism was extended based on kinetics analysis. We propose new pathways that lead to the probable structures. Experimentally measured PIE spectra for several pure components (e.g., C_8 alkenes and cyclic ethers) [34]

were used to verify the present methodology for proposing structures corresponding to measured m/z signals and PIE spectra. To provide additional support to the proposed species, the adiabatic ionization energies (IEs) were calculated using the CBS-QB3 method [53] implemented in Gaussian 09 [54]. This method has been used to calculate the adiabatic IEs of species containing one to three oxygen atoms in the low-temperature oxidation of *n*-butane [41], hexane isomers [33], *n*-heptane [35], and 2,5-dimethylhexane [34]. Recent work by Moshammer et al. [42] on the keto-hydroperoxide formed during dimethyl ether oxidation showed that different conformers need to be considered in the theoretical calculation of species' IEs to correctly interpret the PIE curves. However, it is computationally intractable to compute IEs for all the conformers of species investigated in this work due to the large number of heavy atoms (8–13), possible isomers, and conformers of each isomer. Here, we calculated the IEs of the lowest-energy (zero-point energy) conformer of selected isomers. Geometry optimization was performed at B3LYP/CBSB7 level of theory, followed by a series of high-level single point energy calculations including the complete basis set extrapolation. The estimated uncertainty of the calculated IEs is ±0.05 eV [53], not including the uncertainty from excluding all conformeric structures. Note, the consideration of different conformers might lead to a higher uncertainty than specified [42].

3. Results and discussion

3.1. Classical reaction scheme

Figure 1 presents an overview mass spectrum in the range of m/z = 80–200 which was obtained during DMH oxidation at 510 K (±20 K) and a photon energy of 9.5 eV. These conditions were chosen because the initial oxidation intermediates reach their maximum concentration at 510 K, while fragmentation is minimized at 9.5 eV. The spectrum in Fig. 1 displays signals at m/z ratios of 112.14, 128.13, and 160.11. Despite the mass spectrometer's high mass resolution, a unique determination of the C/H/O composition by exact mass is not possible. Therefore, the molecular formulas proposed for specific m/z signals must be judiciously determined based on mechanistic and kinetic analyses.

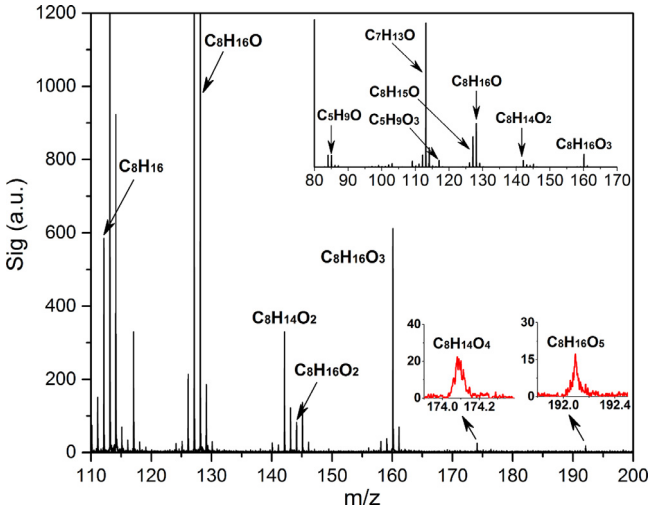

Fig. 1. Mass spectra taken at a photon energy of 9.5 eV during the oxidation of DMH at 510 K. The peaks discussed in this work are labeled with their molecular formula. The peaks of $C_8H_{14}O_4$ and $C_8H_{16}O_5$ are magnified to present the mass resolution. The upper inset presents the mass spectra in the range of m/z 80–170, highlighting intermediates with one to three oxygen atoms, and selected fragments $C_8H_{15}O$, $C_5H_9O_3$, $C_7H_{13}O$ and C_5H_9O.

Simulations for DMH oxidation under the present JSR conditions using the detailed chemical kinetic model of Sarathy et al. [55] demonstrate that high molecular weight intermediates are produced via the classical low-temperature oxidation mechanism (i.e., radical plus O_2 reactions, concerted eliminations, etc.). We postulate that the measured m/z signals correspond to molecular formulas for C_8 alkenes (C_8H_{16}, 112.13 u), cyclic ethers ($C_8H_{16}O$, 128.12 u) and keto-hydroperoxides ($C_8H_{16}O_3$, 160.11 u), respectively. The classical low-temperature reaction pathways producing these intermediates are presented in Scheme S1 in the SI.

The auto-oxidation of DMH is initiated via H-atom abstraction, primarily by OH radicals, to produce three distinct fuel radicals. The initial distribution of primary, secondary and tertiary fuel radicals at 510 K is approximately 26%, 41%, and 33% based on the site-specific OH radical H-atom abstraction rate coefficients proposed by Badra and Farooq [56] and Sivaramakrishnan and Michael [57] (Fig. S2). The subsequent addition of O_2 to primary, tertiary, and secondary fuel radicals, as shown in Scheme S1, leads to three distinct ROO radicals (Note: R = C_nH_{2n+1}), denoted ROO1, ROO2, and ROO3, respectively. These ROO radicals can undergo concerted elimination of HO_2 via 5-membered ring transition states (TS) [58–60] to generate 2,5-dimethylhex-1-ene (C_8H_{16}-1), 2,5-dimethylhex-2-ene (C_8H_{16}-2), and 2,5-dimethylhex-3-ene (C_8H_{16}-3). This is the classical low-temperature chain-terminating pathway (because HO_2 is a weakly reacting radical, its formation tends to inhibit the path to auto-ignition). Figure 2a presents PIE spectra of C_8H_{16} from 8.0 to 9.6 eV. The onset at 8.5 eV in our measured spectra is consistent with the experimentally measured IE of 2,5-dimethylhex-2-ene (8.45 eV [34]). A three-parameter fitting of the measured PIE spectra from the absolute photoionization cross sections of 2,5-dimethylhex-1-ene, 2,5-dimethylhex-2-ene, and 2,5-dimethylhex-3-ene (from Ref. [34]) reveals an isomeric distribution of ~38% 2,5-dimethylhex-1-ene, ~51% 2,5-dimethylhex-2-ene and ~11% 2,5-dimethylhex-3-ene.

In competition with concerted elimination is ROO radical intramolecular H-atom migration via five-, six-, seven-, and eight-membered-ring TS to produce β-QOOH, γ-QOOH, δ-QOOH, and ε-QOOH, respectively (Note: Q = C_nH_{2n}; hereafter, the position of a carbon bonded to an –OOH group in a QOOH radical is denoted as α, β, γ, δ, ε, respectively; α position is the carbon site with the radical). The formation of QOOH radicals ultimately leads to radical chain propagation and/or branching. High-pressure-limit rate rules determined from computational chemistry by Villano et al. [61] (Fig. S3) indicate that the most feasible isomerization routes are via six- and seven-membered-ring TS. Isomerizations with less than six members in the TS have high ring strain energies, while those with greater than seven members in the TS are entropically unfavored. Therefore, assuming that the high-pressure rate constants are valid at these atmospheric pressure experiments, the following analyses only consider intermediate species formed via six- and/or seven-membered ring TS isomerizations.

In the classical low-temperature oxidation scheme, QOOH radicals can react to form a cyclic ether (CE) and an OH radical, which is an important radical chain-propagation route. The atmospheric reaction of isoprene can also produce cyclic ethers, which have been linked to the formation of secondary organic aerosols (SOA) [2,3,62,63]. The four most probable cyclic ethers (Scheme S1) based on our analysis and previous study of DMH [55] are 2-*iso*-butyl-3-methyl-oxetane (CE-1, IE: 9.21 eV [34]), 2-*iso*-propyl-4-methyl-tetrahydrofuran (CE-2, IE: 8.93 eV [34]), 2-*iso*-propyl-4,4-dimethyl-oxetane (CE-3, IE: 9.09 eV [34]), and 2,2,5,5-tetramethyl-tetrahydrofuran (CE-4, IE: 8.93 eV [34]). Previous study showed that substantial 2,2,5,5-tetramethyl-tetrahydrofuran was produced in DMH JSR and flow reactor oxidation [34,55]. The measured IE for 2,2,5,5-tetramethyl-tetrahydrofuran by Rotavera and coworkers [34] is 8.81 eV, which is slightly lower than their calculated IE of 8.93 eV [34]. The measured PIE spectra of $C_8H_{16}O$ by Rotavera and coworkers [34] at 550 K are presented in

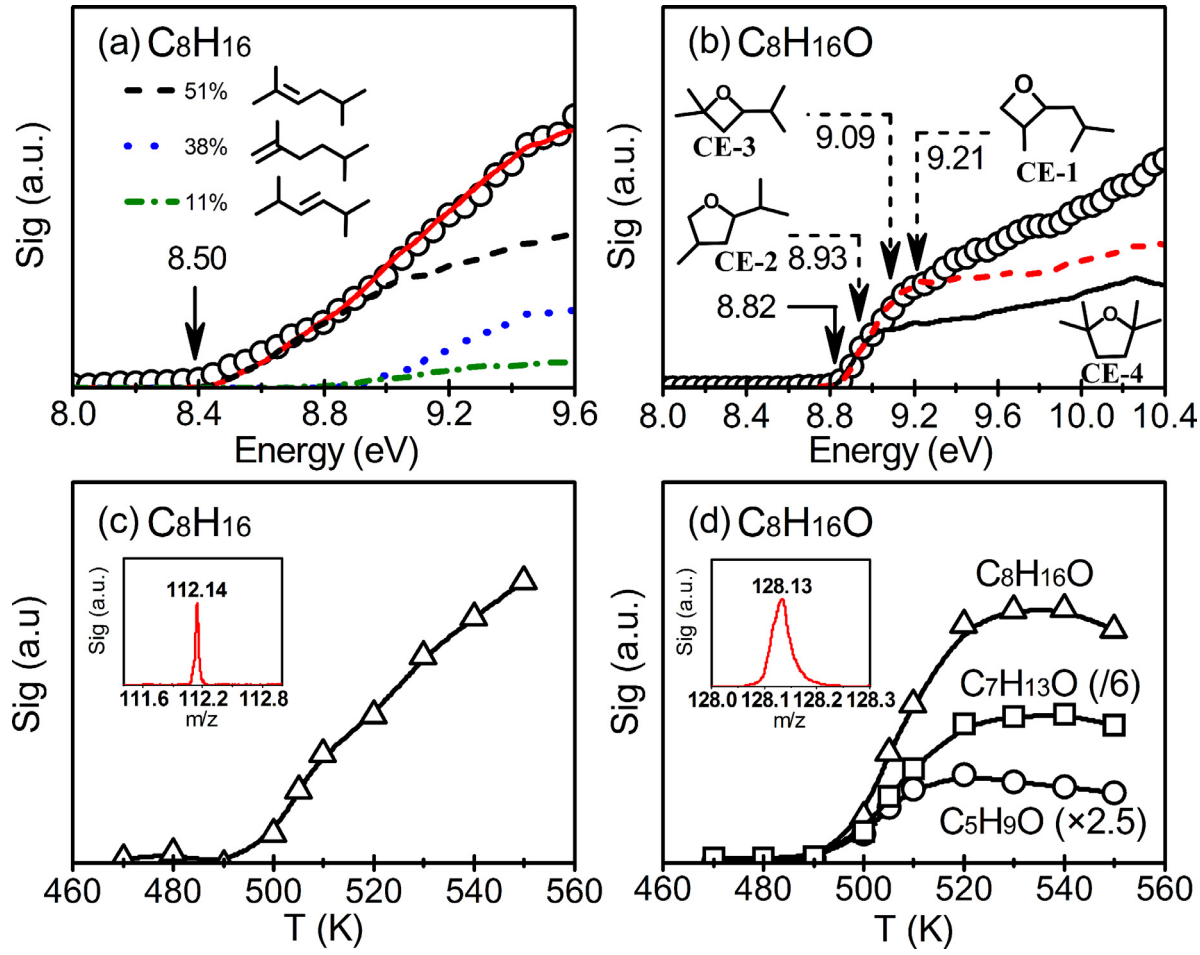

Fig. 2. (Upper panel) Photoionization energy scan of (a) *m/z* 112.14 (C_8H_{16}) and (b) *m/z* 128.13 (C_8H1_6O) produced from DMH low-temperature oxidation at 505 K. The solid arrow in panels (a) and (b) indicates the ionization energy threshold. Panel (a) shows a three parameter fitting for the isomeric distribution of the three C_8H_{16} alkenes, while (b) shows the scaled absolute photoionization spectra of 2,2,5,5-tetramethyl-tetrahydrofuran (black solid line), measured PIE spectra of $C_8H_{16}O$ by Rotavera and coworkers [34] at 550 K (red dashed line), and IEs for other three cyclic ethers (dashed arrows). (Lower panel) The JSR temperature-dependent signal profiles for C_8H_{16} (c) and $C_8H_{16}O$ (d) and its potential fragments ($C_7H_{13}O$ and C_5H_9O) produced from DMH low-temperature oxidation measured at a photon energy of 9.5 eV. The signals of $C_7H_{13}O$ and C_5H_9O are rescaled by the bracketed values. The insets in (c) and (d) are magnified mass peaks of C_8H_{16} and $C_8H_{16}O$, respectively. (For interpretation of the references to color in this figure legend, the reader is referred to the web version of this article.)

Fig. 2b (red dashed line), and is in good agreement with the total PIE curve measured in this work up to 9.2 eV. Figure 2b (black solid line) shows that the scaled absolute PIE spectra for 2,2,5,5-tetramethyl-tetrahydrofuran (CE-4) from Rotavera et al. [34] matches our measured PIE spectra at *m/z* 128.13 from its onset up to 9.0 eV, confirming the presence of this species in our experiments. The discrepancy above 9.0 eV indicates the presence of other cyclic ethers, such as CE-1, CE-2 and/or CE-3. The presence of these four cyclic ethers is further confirmed by their fragments. The inset of Fig. 1 presents a very high signal of $C_7H_{13}O$, which potentially comes from the CH_3 loss from ionization of the cyclic ethers; another mass peak is C_5H_9O, potentially fragmented from CE-1, CE-2, and/or CE-3 via the loss of C_3H_7. The signal profiles of *m/z* 113.11 ($C_7H_{13}O$, 113.10 u) and *m/z* 85.08 (C_5H_9O, 85.07 u) as a function of temperature, shown in Fig. 2d, are similar to that of $C_8H_{16}O$. These observations are in agreement with the results from Rotavera and coworkers [34].

The low-temperature chain branching sequence proceeds via the reaction of QOOH radicals with molecular oxygen (i.e., the second O_2 addition) to form OOQOOH radicals, which subsequently undergo intramolecular H-atom migration to form HOOQ′OOH (Note: Q′ = C_nH_{2n-1}) radical. In the classical low-temperature oxidation scheme, it is often assumed that hydrogen atoms from the carbon bonded to the hydroperoxy group (–OOH) are abstracted, which is plausible because given their lower C–H bond strength of ~3 kcal/mol compared to normal primary, secondary, and tertiary C–H bonds. The HOOQ′OOH is an α-hydroperoxyalkylhydroperoxy radical, which is unstable and easily decomposes to a keto-hydroperoxide (KHP) and an OH radical [64]. Moreover, the keto-hydroperoxide has a weak O–O bond, which can break to generate more OH radicals, thereby acting as a radical chain-branching intermediate.

Figure 1 displays a mass peak with *m/z* 160.11, which corresponds to the molecular formula of KHPs ($C_8H_{16}O_3$, 160.11 u) produced from DMH oxidation. The JSR temperature-dependent signal profile of $C_8H_{16}O_3$ in Fig. 3a displays a sharp increase from 480 to 510 K followed by a rapid decrease. This profile shape is similar to that of KHPs observed in the JSR low-temperature oxidation of *n*-butane [38], hexane isomers [33], and *n*-heptane [35]. Based on the detailed reaction Scheme S1, there are three probable KHPs, specifically, 2,5-dimethyl-3-hydroperoxy-hexanal (KHP-1), 2,5-dimethyl-4-hydroperoxy-hexanal (KHP-2) and 2,5-dimethyl-5-hydroperoxy-hexan-3-one (KHP-3). The formation of these KHPs is linked to specific fuel radicals (i.e., KHP-1 and KHP-2 are from QOOH1-OO3 and QOOH1-OO4 originated from the primary fuel radical, while KHP-3 is generated from QOOH3-OO5 derived from the secondary fuel radical). The tertiary fuel radical cannot lead to a $C_8H_{16}O_3$ KHP because there are no available H-atoms after formation of an OOQOOH radical. The calculated IEs for KHP-1, KHP-2 and KHP-3 are 9.60, 9.21, and 8.75 eV, respectively. The onset at 8.8 eV for *m/z* 160.11

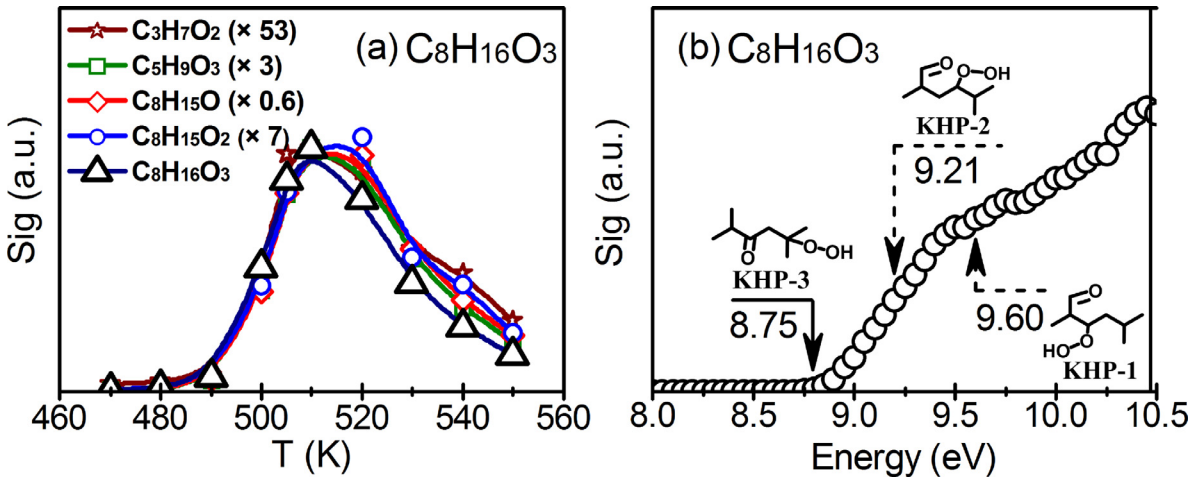

Fig. 3. (a) JSR temperature-dependent signal profiles of m/z 160.11 ($C_8H_{16}O_3$) and its potential fragments ($C_8H_{15}O_2$, $C_8H_{15}O$, $C_5H_9O_3$, and $C_3H_7O_2$) from DMH low-temperature oxidation measured at a photon energy of 9.5 eV. The fragment signals are normalized by the $C_8H_{16}O_3$ signal at 510 K. The normalization ratios are presented in the brackets. (b) Photoionization energy scan of $C_8H_{16}O_3$ produced from DMH low-temperature oxidation at 505 K. The solid arrow indicates the calculated ionization energy threshold for KHP-3; the dashed arrows indicate the calculated IEs of the other two probable KHP isomers.

($C_8H_{16}O_3$) in Fig. 3b is consistent with the calculated IE of KHP-3. Previous kinetic modeling work [55] has shown that KHP-3 is the most significant isomer produced during DMH low-temperature oxidation. KHP-1's IE is considerably higher than the observed onset for $C_8H_{16}O_3$, but simulations [55] predict that this isomer is also produced in significant amounts. The inset of Fig 1. shows several peaks corresponding to possible ionization fragments of KHP-3 via the scission of CO–OH ($C_8H_{15}O_2$, 143.11 u), C–OOH ($C_8H_{15}O$, 127.11 u), C_3H_7–$C_5H_9O_3$ ($C_5H_9O_3$, 117.06 u), $C_3H_7O_2$–C_5H_9O ($C_3H_7O_2$, 75.04 u, not presented in Fig. 1) bonds. Figure 3a shows that these fragments have similar JSR temperature-dependent signal profiles as KHP-3.

3.2. Extended reaction scheme

The mass spectra in Fig. 1 depicts peaks with m/z 174.09 and 192.09. These two high molecular weight species produced from DMH oxidation are postulated to have molecular formulas of $C_8H_{14}O_4$ (174.09 u) and $C_8H_{16}O_5$ (192.10 u), respectively. Highly oxidized multifunctional molecules (HOM) with multiple carbonyl and hydroperoxy functional groups have been previously observed and identified as ELVOCs during the ozonolysis of cycloalkenes, alkenes, and olefinic aldehydes [5,6,65]. In atmospheric chemistry, ELVOCs may condense to generate low volatility SOA [1], which affect the Earth's radiation balance [66]. The formation mechanism of HOMs is initiated by alkylperoxy radicals (ROO) isomerization through intramolecular H-atom abstraction reactions, followed by sequential O_2 addition steps [1,4,5]. The species with multiple carbonyl and hydroperoxy functional groups have only been seldom reported under combustion related conditions [67], and never by direct sampling methods. The temperature-dependent signal profiles of $C_8H_{14}O_4$ and $C_8H_{16}O_5$ shown in Fig. 4 are similar to that of $C_8H_{16}O_3$, thus implicating them as alternative intermediates in the low-temperature oxidation mechanism.

The classical low-temperature oxidation scheme considers the formation of species with up to three oxygen atoms, and thus cannot explain the production of $C_8H_{14}O_4$ and $C_8H_{16}O_5$ species detected in this work. Secondary radical–radical reactions could produce $C_8H_{16}O_5$ and $C_8H_{14}O_4$ species, as well as other $C_xH_yO_z$ species with similar m/z values, but such pathways are only significant at higher radical concentrations that can occur following KHPs decomposition at higher temperature. Radical–radical processes, such as those initiated by oxidation of *iso*-butene, known to be a product of initial oxidation steps of DMH [34], were explored in chemical

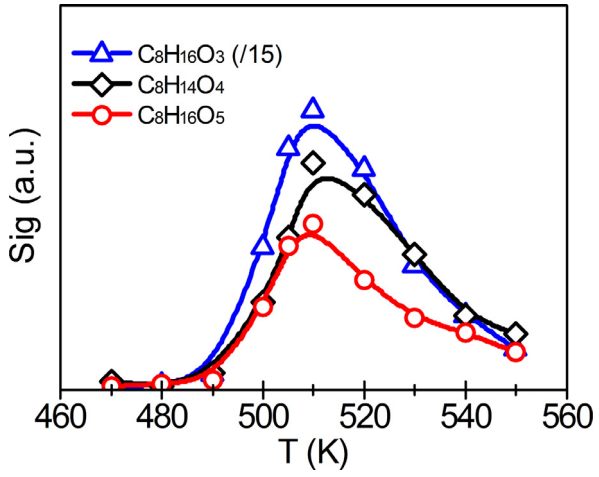

Fig. 4. JSR temperature-dependent signal profiles of $C_8H_{16}O_3$, $C_8H_{14}O_4$, and $C_8H_{16}O_5$ from DMH low-temperature oxidation measured at a photon energy of 9.5 eV. The signal of $C_8H_{16}O_3$ (KHP) is divided by 15.

kinetic modeling simulations [55] and shown to be negligible. In the present experiments, $C_8H_{14}O_4$ and $C_8H_{16}O_5$ species are detected at temperatures comparable to those where KHPs are observed, so it is unlikely that decomposition of KHPs and secondary radical–radical reactions lead to their production. The m/z of $C_8H_{16}O$ (cyclic ethers), $C_8H_{16}O_3$ (keto-hydroperoxides), and $C_8H_{16}O_5$ increases by increments of 32 Da. The former two species are produced by first and second O_2 addition reactions to form QOOH and OOQOOH, respectively, followed by the release of an OH radical. The observation of $C_8H_{16}O_5$ suggests a third O_2 addition process. Herein, we propose the reaction scheme to produce $C_8H_{16}O_5$, i.e., OOQOOH intramolecular H-migration, subsequent O_2 addition, isomerization, and OH release.

The classical reaction scheme discussed above shows that the OOQOOHs from the primary fuel radical, i.e., QOOH1–OO3 and QOOH1–OO4, produce KHP-1 and KHP-2 via the isomerization to HOOQ′OOH. However, these OOQOOH radicals can also undergo intramolecular H-atom migration from a non-COOH site, denoted as an "alternative isomerization" here. To be distinct from the HOOQ′OOH produced from the classical scheme, a $P(OOH)_2$ (Note: $P = C_nH_{2n-1}$) [68] was selected to denote the alternative isomerization products.

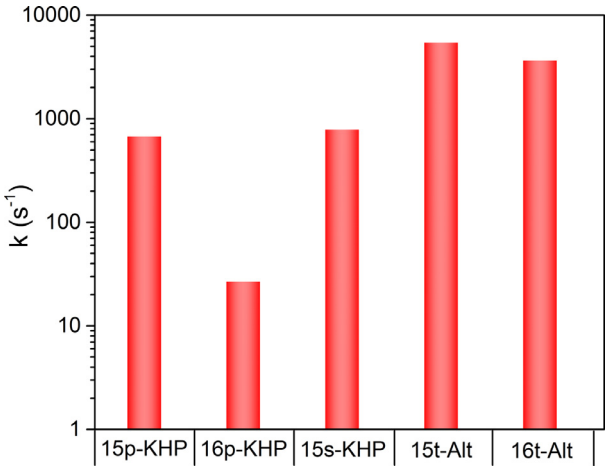

Fig. 5. Selected high-pressure-limit rate constants of OOQOOH decomposition to KHP and isomerization to $P(OOH)_2$ at 510 K. 15p-KHP denotes the OOQOOH decomposition to KHP via a six-membered-ring TS intramolecular H-atom migration from a primary C-OOH site. 15t-Alt denotes an OOQOOH isomerization to $P(OOH)_2$ via a six-membered-ring TS intramolecular H-atom migration from a normal tertiary C–H. The rate constants of OOQOOH decomposition to KHP from Sharma et al. [64] are averaged values.

It should be noted that $P(OOH)_2$ has the same molecular formula as HOOQ′OOH, but the radical positions are different. In several cases, as discussed below, this pathway is competitive to the intramolecular H-atom migration leading to a keto-hydroperoxide. Figure 5 presents the comparison of selected high-pressure-limit rate constants of OOQOOH decomposition to KHP and alternative isomerization to $P(OOH)_2$. The rate constants of OOQOOH isomerization to $P(OOH)_2$, e.g., 15t-Alt and 16t-Alt, and OOQOOH decomposition to KHP are based on calculations by Sharma et al. [64]. Recent work by Bugler and coworkers [69] on the ignition of three pentane isomers showed that using the rate constants by Sharma et al. [64] predicts well the measured ignition delay times. Figure 5 clearly indicates that the rate constants of 15p-KHP, 16p-KHP, and 15s-KHP are slower than 15t-Alt and 16t-Alt, suggesting the feasibility of the alternative isomerization of OOQOOH isomerization to $P(OOH)_2$. Similar conclusions on the relative importance of alternative isomerization can be drawn using isomerization rate rules from calculations by Villano et al. [61] and Miyoshi [68].

Scheme 2 presents the alternative isomerization reaction mechanism for two OOQOOH radicals derived from a primary fuel radical. In Scheme 2a, the alternative isomerization of QOOH1-OO3 produces POOH13e. This is a γ,ε-$P(OOH)_2$ radical (hereafter, the position of a carbon bonded to an –OOH group in a $P(OOH)_2$ radical is designated by α, β, γ, δ, ε, respectively; α position is the carbon site with the radical). Miyoshi's calculations [68] show that $P(OOH)_2$ radicals can cyclize to form hydroperoxy cyclic ethers (HPCE) with three, four, five, or six-membered rings (as shown in Scheme 2). The molecular formula of an HPCE ($C_8H_{16}O_3$, 160.11 u) is identical to that of a KHP, suggesting that the signal measured at m/z 160.11 could also include HPCEs. We are unable to definitively distinguish between HPCE and KHP, since they are isomers and their photoionization energies are unknown. We note that previous work on the detection of KHPs during the oxidation of *n*-butane [38] and *n*-heptane [35] may have included HPCEs contributing to the same m/z signal. Battin–Leclerc's work on *n*-butane [41] stated that the HPCEs at the same mass as the KHPs were not important based on kinetic modeling results.

Furthermore, C–O β-scission of a β,γ-$P(OOH)_2$ radical, POOH14b in Scheme 2b produces an olefinic hydroperoxide ($C_8H_{16}O_2$, OHP, 144.12 u) and an HO_2 radical. In Fig. 1, a mass peak with m/z 144.12 corresponding to the molecular weight of $C_8H_{16}O_2$ is observed, which alludes to the production of olefinic hydroperoxides via the aforementioned scheme. The concerted elimination of HO_2 from OOQOOH also produces OHP, but such channels are expected to be less important at the temperature range studied here.

Additional calculations by Miyoshi [68] indicate $P(OOH)_2$ radicals can undergo O_2 addition at low temperatures (e.g., 510 K in this work). In Scheme 2a, the third O_2 addition intermediate,

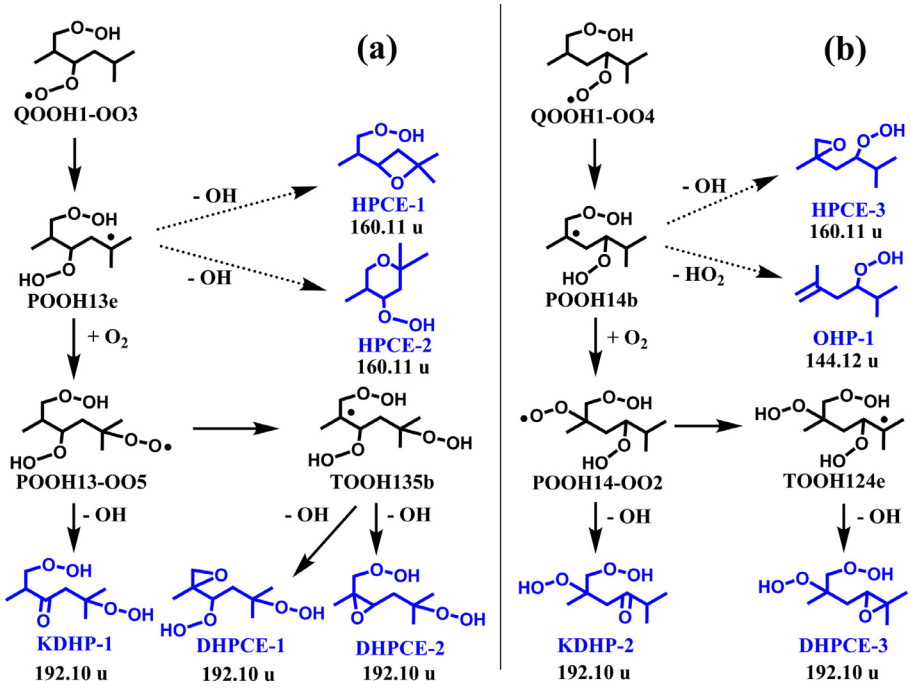

Scheme 2. The reaction network of alternative isomerization of OOQOOH from the primary fuel radical. The most feasible pathways are presented. The subsequent reactions following the solid arrows, i.e., O_2 addition, intramolecular H-abstraction, and decomposition produce $C_8H_{16}O_5$ species; the decomposition of $P(OOH)_2$, dashed arrows, leads to hydroperoxy cyclic ethers and olefinic hydroperoxides.

POOH13-OO5, undergoes intramolecular H-atom migration from the γ-C–H bonded to the OOH group, via a six-membered-ring TS, to produce a keto-dihydroperoxide (KDHP) and an OH radical. On the other hand, alternative isomerization of POOH13-OO5 via a seven-membered-ring TS intramolecular H-atom migration from the tertiary C–H generates an intermediate with three hydroperoxy functional groups, TOOH135b. Figure S4 presents the averaged high-pressure-limit rate constant for the decomposition of β-QOOH, γ-QOOH, δ-QOOH and ε-QOOH radicals to form a cyclic ether and an OH radical at 510 K [70]. Based on comparison of those rates, it is plausible that TOOH135b decomposes to dihydroperoxy cyclic ether (DHPCE) (i.e., oxirane with a three-membered ring). Scheme 2b presents a similar scheme for the QOOH1-OO4 radical.

OOQOOH radicals derived from the tertiary fuel radical, i.e. QOOH2-OO4 and QOOH2-OO5 in Scheme S1, can also undergo a series of alternative isomerization and reactions similar to those presented in Scheme 2. The most feasible pathways presented in Scheme S2 and denoted with solid arrows produce $C_8H_{16}O_5$ isomers (i.e., KDHPs and DHPCEs). Compared to the classical low-temperature oxidation scheme, these pathways are important for branched alkane auto-oxidation because they divert the carbon flux towards more reactive intermediates. Scheme S3 presents the reaction network of alternative isomerization of OOQOOH derived from the secondary fuel radical, e.g., QOOH3-OO5. The most probable $C_8H_{16}O_5$ isomers produced from this reaction network are DHPCEs.

Table 1 presents the calculated adiabatic ionization energies of the probable KDHP and DHPCE isomers from Scheme 2. The IEs of other probable isomers produced from Schemes S2 and S3 are presented in Table S1 in the SI. The calculated IE of KDHP-2 (9.04 eV) is consistent with the experimental onset for m/z 192.09 ($C_8H_{16}O_5$) at 9.0 eV in Fig. 6a, while that of KDHP-1 (9.33 eV) is higher. The calculated IEs of DHPCEs are in the range of 8.9–9.24 eV, with eight of them located within 0.1 eV of the measured IE onset. It should be noted that due to large numbers of conformers, the isomeric assignment may change if all conformeric effects are taken into account.

A mass peak with m/z 159.11 is observed (see Fig. 1), which corresponds to the molecular weight of $C_8H_{15}O_3$ (159.10 u). The JSR temperature-dependent signal profile of $C_8H_{15}O_3$ in the inset of Fig. 6b is similar to that of $C_8H_{16}O_5$. We explored the possibility of $C_8H_{15}O_3$ being an ionization fragment of $C_8H_{16}O_5$. Calculations of the appearance energies for various fragmentation pathways show that the ionized $C_8H_{16}O_5$ species can undergo HO_2 loss to produce $C_8H_{15}O_3$. The HO_2 loss pathway from ionized KDHP-1, potentially an important $C_8H_{16}O_5$ isomer, was calculated in this work (Fig. S5). The calculated appearance energy (AE) of $C_8H_{15}O_3$ is 9.41 eV, which is consistent with the measured AE of 9.4 eV in Fig. 6b.

The $C_8H_{15}O_3$ signal could also come from the loss of H atoms from ionized KHP species ($C_8H_{16}O_3$). To investigate the latter's

Table 1
The structures and ionization energies of the probable isomers of $C_8H_{16}O_5$ and $C_8H_{14}O_4$ produced from Schemes 2 and 3. The calculation is at CBS-QB3 level.

Formula and u	Species	Structure	IE (eV)
$C_8H_{16}O_5$ 192.10	KDHP-1	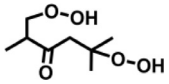	9.33
	KDHP-2	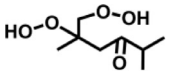	9.04
	DHPCE-1	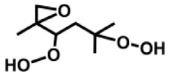	9.09
	DHPCE-2	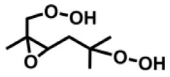	9.06
	DHPCE-3	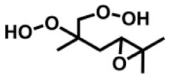	9.10
$C_8H_{14}O_4$ 174.09	DKHP-1	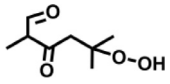	9.14
	DKHP-2	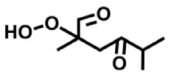	9.03
	KHPCE-1	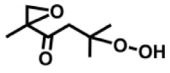	9.12
	KHPCE-2	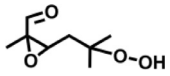	9.50
	KHPCE-3	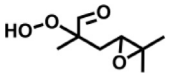	9.00

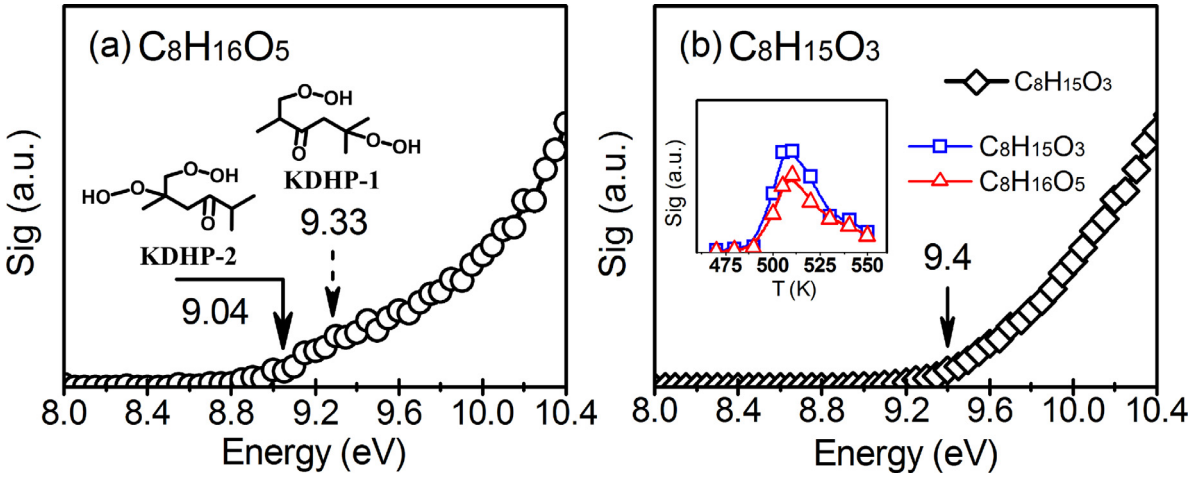

Fig. 6. (a) Photoionization energy scan of m/z 192.09 ($C_8H_{16}O_5$) produced from DMH low-temperature oxidation at 505 K. The solid arrow indicates the calculated ionization energy threshold for KDHP-2; the dashed arrow indicates the calculated IE of KDHP-1. The other probable $C_8H_{16}O_5$ isomers in Tables 1 and S1 are not presented. (b) Photoionization energy scan of m/z 159.11 ($C_8H_{15}O_3$), which can be a fragment of ionized $C_8H_{16}O_5$ via the loss of HO_2. The measured appearance energy threshold is 9.4 eV. The inset is the JSR temperature-dependent signal profiles of $C_8H_{16}O_5$ and $C_8H_{15}O_3$ from DMH low-temperature oxidation measured at a photon energy of 9.5 eV.

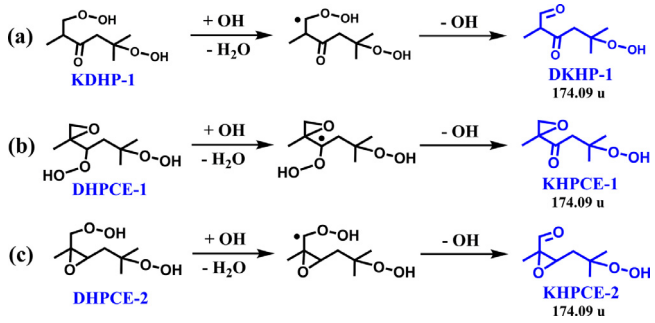

Scheme 3. The reaction network of $C_8H_{14}O_4$ species, DKHP-1, KHPCE-1, and KHPCE-2 from $C_8H_{16}O_5$ species of KDHP-1, DHPCE-1, and DHPCE-2 in Scheme 2a.

contribution to the $C_8H_{15}O_3$ signal, the AE of the dissociation products from KHP-3 were calculated. The AEs of $C_8H_{15}O_3$ from the H-loss of ionized KHP-3 are in the range of 10.3–12.7 eV. These values are far from the measured onset of 9.4 eV, so are not expected to contribute to the temperature-dependent signal of $C_8H_{15}O_3$ at 9.5 eV.

Previous studies on *n*-heptane oxidation [35,71] have shown that KHPs undergo H-abstraction from the C–H attached to the OOH group, and then dissociate easily to diketo-compounds, such as 2,4-heptanedione ($C_7H_{12}O_2$). In this work, species with a molecular formula of $C_8H_{14}O_2$ (*m*/*z* 142.11) were also observed during DMH oxidation, as shown in Fig. 1. The JSR temperature-dependent signal profile of this species, as well as the energy scan are presented in Fig. S6. Analogous to diketone production from KHPs, H-atom abstraction from $C_8H_{16}O_5$ species followed by β-scission can result in the formation of diketo-hydroperoxides (DKHPs)/keto-hydroperoxy cyclic ethers (KHPCEs). Scheme 3 presents examples for the formation of a diketo-hydroperoxide (DKHP-1) and two keto-hydroperoxy cyclic ethers (KHPCE-1 and KHPCE-2).

The calculated IEs of the DKHP and KHPCE isomers produced from the $C_8H_{16}O_5$ species in Scheme 2 are presented in Table 1. The IEs for other probable $C_8H_{14}O_4$ isomers produced from other $C_8H_{16}O_5$ species in Scheme S2 and S3 are given in Table S1 in the SI. Figure 7a presents the measured PIE curve of *m*/*z* 174.09 ($C_8H_{14}O_4$) from 8.0 to 10.4 eV. The calculated IEs of DKHP-1 and DKHP-2 are 9.14 and 9.03 eV, respectively, while those of KHPCEs are in the range of 8.71–9.72 eV. The IE of KHPCE-10 (8.71 eV) is consistent with the experimental onset for *m*/*z* 174.09 at 8.7 eV; the full interpretation of the PIE curve requires a complete Franck–Condon factor analysis of many isomeric and conformeric structures and is beyond the scope of the paper. Similar to $C_8H_{16}O_5$ species, the potential fragmentation via the HO_2 loss of ionized $C_8H_{14}O_4$ species is also observed, i.e., *m*/*z* 141.11 corresponding to $C_8H_{13}O_2$ (141.09 u) in Fig. 1. The inset of Fig. 7b shows that the JSR temperature-dependent signal of $C_8H_{13}O_2$ is similar to that of $C_8H_{14}O_4$. Figure S7 presents the calculated pathway of DKHP-1 to $C_8H_{13}O_2$ via HO_2 loss, which is similar to that of KDHP-1 ionization to $C_8H_{15}O_3$. The calculated AE is 9.30 eV, consistent with the measured onset at 9.35 eV in Fig. 7b.

The calculated IEs in Table 1 and S1 show that all probable $C_8H_{16}O_5$ isomers (i.e., KDHPs and DHPCEs) derived from the reaction scheme proposed in this work could contribute to the signal of *m*/*z* 192.09 at 9.5 eV. Similarly, many $C_8H_{14}O_4$ isomers (i.e., DKHPs and KHPCEs), derived from $C_8H_{16}O_5$ species likely contribute to the signal of *m*/*z* 174.09 at 9.5 eV. The observed fragmentation patterns and selected AE calculations are also consistent with the proposed $C_8H_{16}O_5$ and $C_8H_{14}O_4$ structures. A detailed exploration of possible $C_8H_{16}O_5$ and $C_8H_{14}O_4$ isomers containing multiple carbonyl and/or hydroxyl functional groups was not considered here, although some of those isomers could also be consistent with the observed photoionization spectra. However, such species are difficult to produce, as they require radical–radical recombination reactions that are not favored at the reactor conditions studied here [55]. Thus, the observed early decomposition of the $C_8H_{16}O_5$ and $C_8H_{14}O_4$ species is further evidence that these are highly unstable KDHPs, DHPCEs, DKHPs and KHPCEs species.

The above mentioned schemes show that the formation of $C_8H_{16}O_5$ and $C_8H_{14}O_4$ species is accompanied by the release of an OH radical. Furthermore, these species, regardless of their exact structure (e.g., KDHP, DHPCE, DKHP, and KHPCE), contain one or two hydroperoxy groups, whose homolytic O–O scission releases another OH radical. The reactions associated with production and consumption of $C_8H_{16}O_5$ and $C_8H_{14}O_4$ species result in a net increase of OH radical production, and thus these are radical chain-branching pathways. The present work's detection of these HOM species indicates that an extended reaction scheme exists for 2,5-dimethylhexane, as shown in Scheme 4. The pathways to hydroperoxy cyclic ether and olefinic hydroperoxide are also included. The extended reaction scheme is expected to exist for other straight and branched alkanes with sufficiently long carbon chains.

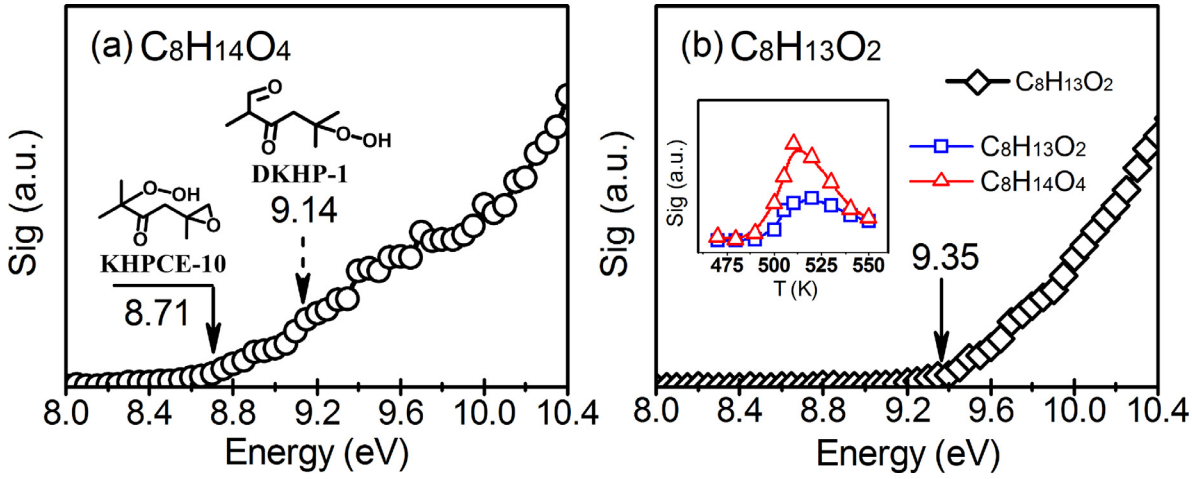

Fig. 7. (a) Photoionization energy scan of *m*/*z* 174.09 ($C_8H_{14}O_4$) produced from DMH low-temperature oxidation at 505 K. The solid arrow indicates the calculated ionization energy threshold for KHPCE-10 in Table S1; the dashed arrow indicates the calculated IE of DKHP-1. The other probable $C_8H_{14}O_4$ isomers in Tables 1 and S1 are not presented. (b) Photoionization energy scan of *m*/*z* 141.11 ($C_8H_{13}O_2$), which could be a fragment of ionized $C_8H_{14}O_4$ via the loss of HO_2. The measured appearance energy threshold is 9.35 eV. The inset is the JSR temperature-dependent signal profiles of $C_8H_{14}O_4$ and $C_8H_{13}O_2$ from DMH low-temperature oxidation measured at a photon energy of 9.5 eV.

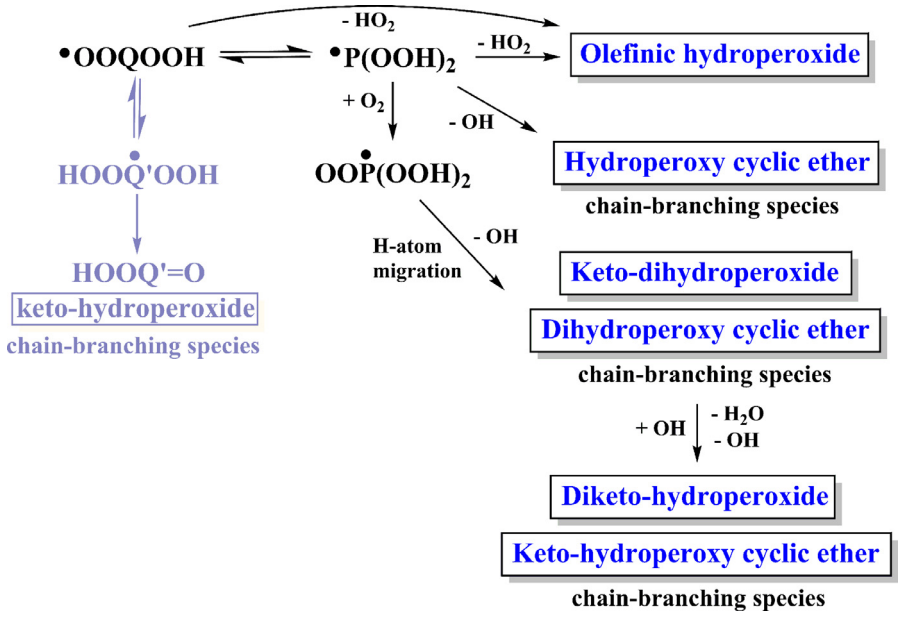

Scheme 4. Extended scheme for 2,5-dimethylhexane low-temperature oxidation. The scheme starts from the OOQOOH radical, whose upstream reactions are presented in Scheme 1. The important intermediates are highlighted.

4. Conclusions

In this work, several key intermediates controlling the low-temperature oxidation reactivity of 2,5-dimethylhexane, especially highly oxidized multifunctional species, were observed and their reaction mechanism was elucidated. The detection of C_8 alkenes, cyclic ethers, and keto-hydroperoxides supports the classical low-temperature oxidation scheme of hydrocarbons. In addition, C_8 species with four and five oxygen atoms were identified as multifunctional molecules containing hydroperoxy and carbonyl/ether functional groups. The detection of these species suggests that a third O_2 addition process exists at combustion relevant conditions, indicating the presence of previously unconsidered radical chain-branching pathways.

The work demonstrates that low-temperature radical chain-branching reactions are significantly more complex than traditionally conceptualized and applied. This creates new research avenues in low-temperature oxidation, which has implications on classical problems such as fuel ignition, atmospheric gas-phase chemistry, and the oxidative stability of liquid hydrocarbons.

Acknowledgments

This work was initiated by the Clean Combustion Research Center with funding from King Abdullah University of Science and Technology (KAUST) and Saudi Aramco under the FUELCOM program. Research reported in this publication was also supported by competitive research funding from KAUST. L.D.Z. is grateful for the support from National Key Scientific Instruments and Equipment Development Program of China (2012YQ22011305). The work of N.H., K.M., and C.A.T. was supported by the U.S. Department of Energy, Office of Science, Office of Basic Energy Sciences. D.M.P.V. and S.R.L. are supported by the Department of Energy Gas Phase Chemical Physics Program at Lawrence Berkeley National Laboratory, under contract DEAC02-05CH11231. D.M.P.V. is particularly grateful to the Alexander von Humboldt Foundation for a Feodor Lynen fellowship and she greatly acknowledges the technical support by James Breen, Erik Granlund and William Thur during the designing process and the fabrication of the JSR system. C.H. and K.K.H. are grateful for partial support by DFG within the large-scale research structure SFB 686, TP B3. P.D. has received funding from the European Research Council under the European Community's Seventh Framework Programme (FP7/2007-2013)/ERC grant agreement no. 291049-2G-CSafe. Sandia is a multi-program laboratory operated by Sandia Corporation, a Lockheed Martin Company, for the National Nuclear Security Administration under contract DE-AC04-94-AL85000. The Advanced Light Source is supported by the Director, Office of Science, Office of Basic Energy Sciences, of the U.S. Department of Energy under Contract No. DEAC02-05CH11231. We would like to thank Prof. Fei Qi for support and helpful discussions, and Lili Xing and Hao Zhao for technical support.

Supplementary materials

Supplementary material associated with this article can be found, in the online version, at doi:10.1016/j.combustflame.2015.11.035.

References

[1] M. Ehn, J.A. Thornton, E. Kleist, M. Sipila, H. Junninen, I. Pullinen, M. Springer, F. Rubach, R. Tillmann, B. Lee, F. Lopez-Hilfiker, S. Andres, I.-H. Acir, M. Rissanen, T. Jokinen, S. Schobesberger, J. Kangasluoma, J. Kontkanen, T. Nieminen, T. Kurten, L.B. Nielsen, S. Jorgensen, H.G. Kjaergaard, M. Canagaratna, M.D. Maso, T. Berndt, T. Petaja, A. Wahner, V.-M. Kerminen, M. Kulmala, D.R. Worsnop, J. Wildt, T.F. Mentel, A large source of low-volatility secondary organic aerosol, Nature 506 (2014) 476–479.

[2] F. Paulot, J.D. Crounse, H.G. Kjaergaard, A. Kürten, J.M. St. Clair, J.H. Seinfeld, P.O. Wennberg, Unexpected epoxide formation in the gas-phase photooxidation of isoprene, Science 325 (2009) 730–733.

[3] M. Claeys, B. Graham, G. Vas, W. Wang, R. Vermeylen, V. Pashynska, J. Cafmeyer, P. Guyon, M.O. Andreae, P. Artaxo, W. Maenhaut, Formation of secondary organic aerosols through photooxidation of isoprene, Science 303 (2004) 1173–1176.

[4] J.D. Crounse, L.B. Nielsen, S. Jørgensen, H.G. Kjaergaard, P.O. Wennberg, Autoxidation of organic compounds in the atmosphere, J. Phys. Chem. Lett. 4 (2013) 3513–3520.

[5] M.P. Rissanen, T. Kurtén, M. Sipilä, J.A. Thornton, J. Kangasluoma, N. Sarnela, H. Junninen, S. Jørgensen, S. Schallhart, M.K. Kajos, R. Taipale, M. Springer, T.F. Mentel, T. Ruuskanen, T. Petäjä, D.R. Worsnop, H.G. Kjaergaard, M. Ehn, The formation of highly oxidized multifunctional products in the ozonolysis of cyclohexene, J. Am. Chem. Soc. 136 (2014) 15596–15606.

[6] M.P. Rissanen, T. Kurtén, M. Sipilä, J.A. Thornton, O. Kausiala, O. Garmash, H.G. Kjaergaard, T. Petäjä, D.R. Worsnop, M. Ehn, M. Kulmala, Effects of chemical complexity on the autoxidation mechanisms of endocyclic alkene ozonolysis products: from methylcyclohexenes toward understanding α-pinene, J. Phys. Chem. A 119 (2015) 4633–4650.

[7] J. Cartlidge, C.F.H. Tipper, Knock resistance and anti-knock with hydrocarbon fuels, Combust. Flame 5 (1961) 87–91.

[8] J. Cartlidge, C.F.H. Tipper, The peroxides formed during hydrocarbon slow combustion and their role in the mechanism, Proc. R. Soc. London, Ser. A 261 (1961) 388–401.
[9] A.R. Burgess, R.G.W. Laughlin, M.I.D. White, Symposium on Gas Kinetics, Szeged, Hungary, 1969, p. 379.
[10] R.W. Walker, C. Morley, Basic chemistry of combustion, in: M.J. Pilling (Ed.), Comprehensive Chemical Kinetics, Low-Temperature Combustion and Autoignition, 35, Elsevier, Amsterdam, 1997 (Chapter 1).
[11] F. Battin-Leclerc, Detailed chemical kinetic models for the low-temperature combustion of hydrocarbons with application to gasoline and diesel fuel surrogates, Prog. Energy Combust. Sci. 34 (2008) 440–498.
[12] J. Zádor, C.A. Taatjes, R.X. Fernandes, Kinetics of elementary reactions in low-temperature autoignition chemistry, Prog. Energy Combust. Sci. 37 (2011) 371–421.
[13] R.A. Cox, J.A. Cole, Chemical aspects of the autoignition of hydrocarbon-air mixtures, Combust. Flame 60 (1985) 109–123.
[14] H. Yin, L. Xu, N.A. Porter, Free radical lipid peroxidation: mechanisms and analysis, Chem. Rev. 111 (2011) 5944–5972.
[15] F. Gugumus, Physico-chemical aspects of polyethylene processing in an open mixer. Part 25: Mechanisms of aldehyde and carboxylic acid formation, Polym. Degrad. Stabl. 91 (2006) 3416–3428.
[16] J. Pfaendtner, L.J. Broadbelt, Mechanistic modeling of lubricant degradation. 1. Structure−reactivity relationships for free-radical oxidation, Ind. Eng. Chem. Res. 47 (2008) 2886–2896.
[17] K.U. Ingold, Inhibition of the autoxidation of organic substances in the liquid phase, Chem. Rev. 61 (1961) 563–589.
[18] K.U. Ingold, D.A. Pratt, Advances in radical-trapping antioxidant chemistry in the 21st century: a kinetics and mechanisms perspective, Chem. Rev. 114 (2014) 9022–9046.
[19] D.E. Hathway, J.W.T. Seakins, Autoxidation of polyphenols. Part III. Autoxidation in neutral aqueous solution of flavans related to catechin, J. Chem. Soc. (1957) 1562–1566.
[20] A.J.S. Angelo, Lipid oxidation in foods, Crit. Rev. Food Sci. 36 (1996) 175–224.
[21] A.C. Davis, J.S. Francisco, Reactivity trends within alkoxy radical reactions responsible for chain branching, J. Am. Chem. Soc. 133 (2011) 18208–18219.
[22] A.C. Davis, J.S. Francisco, Ab initio study of key branching reactions in biodiesel and Fischer–Tropsch fuels, J. Am. Chem. Soc. 133 (2011) 19110–19124.
[23] H.J. Curran, P. Gaffuri, W.J. Pitz, C.K. Westbrook, A comprehensive modeling study of n-heptane oxidation, Combust. Flame 114 (1998) 149–177.
[24] H.J. Curran, P. Gaffuri, W.J. Pitz, C.K. Westbrook, A comprehensive modeling study of iso-octane oxidation, Combust. Flame 129 (2002) 253–280.
[25] M.P. Halstead, L.J. Kirsch, C.P. Quinn, The autoignition of hydrocarbon fuels at high temperatures and pressures—fitting of a mathematical model, Combust. Flame 30 (1977) 45–60.
[26] C.K. Westbrook, F.L. Dryer, Chemical kinetic modeling of hydrocarbon combustion, Prog. Energy Combust. Sci. 10 (1984) 1–57.
[27] J.M. Simmie, Detailed chemical kinetic models for the combustion of hydrocarbon fuels, Prog. Energy Combust. Sci. 29 (2003) 599–634.
[28] S.M. Sarathy, P. Oßwald, N. Hansen, K. Kohse-Höinghaus, Alcohol combustion chemistry, Prog. Energy Combust. Sci. 44 (2014) 40–102.
[29] F. Battin-Leclerc, E. Blurock, R. Bounaceur, R. Fournet, P.-A. Glaude, O. Herbinet, B. Sirjean, V. Warth, Towards cleaner combustion engines through groundbreaking detailed chemical kinetic models, Chem. Soc. Rev. 40 (2011) 4762–4782.
[30] J.D. Savee, E. Papajak, B. Rotavera, H. Huang, A.J. Eskola, O. Welz, L. Sheps, C.A. Taatjes, J. Zádor, D.L. Osborn, Direct observation and kinetics of a hydroperoxyalkyl radical (QOOH), Science 347 (2015) 643–646.
[31] O. Herbinet, F. Battin-Leclerc, Progress in understanding low-temperature organic compound oxidation using a jet-stirred reactor, Int. J. Chem. Kinet. 46 (2014) 619–639.
[32] O. Herbinet, F. Battin-Leclerc, S. Bax, H.L. Gall, P.-A. Glaude, R. Fournet, Z. Zhou, L. Deng, H. Guo, M. Xie, F. Qi, Detailed product analysis during the low temperature oxidation of n-butane, Phys. Chem. Chem. Phys. 13 (2011) 296–308.
[33] Z.D. Wang, O. Herbinet, Z.J. Cheng, B. Husson, R. Fournet, F. Qi, F. Battin-Leclerc, Experimental investigation of the low temperature oxidation of the five isomers of hexane, J. Phys. Chem. A 118 (2014) 5573–5594.
[34] B. Rotavera, J. Zádor, O. Welz, L. Sheps, A.M. Scheer, J.D. Savee, M. Akbar Ali, T.S. Lee, B.A. Simmons, D.L. Osborn, A. Violi, C.A. Taatjes, Photoionization mass spectrometric measurements of initial reaction pathways in low-temperature oxidation of 2,5-dimethylhexane, J. Phys. Chem. A 118 (2014) 10188–10200.
[35] O. Herbinet, B. Husson, Z. Serinyel, M. Cord, V. Warth, R. Fournet, P.-A. Glaude, B. Sirjean, F. Battin-Leclerc, Z.D. Wang, M.F. Xie, Z.J. Cheng, F. Qi, Experimental and modeling investigation of the low-temperature oxidation of n-heptane, Combust. Flame 159 (2012) 3455–3471.
[36] F. Battin-Leclerc, A. Rodriguez, B. Husson, O. Herbinet, P.-A. Glaude, Z. Wang, Z. Cheng, F. Qi, Products from the oxidation of linear isomers of hexene, J. Phys. Chem. A 118 (2014) 673–683.
[37] M. Cord, B. Husson, J.C. Lizardo Huerta, O. Herbinet, P.-A. Glaude, R. Fournet, B. Sirjean, F. Battin-Leclerc, M. Ruiz-Lopez, Z. Wang, M. Xie, Z. Cheng, F. Qi, Study of the low temperature oxidation of propane, J. Phys. Chem. A 116 (2012) 12214–12228.
[38] F. Battin-Leclerc, O. Herbinet, P.-A. Glaude, R. Fournet, Z. Zhou, L. Deng, H. Guo, M. Xie, F. Qi, Experimental confirmation of the low-temperature oxidation scheme of alkanes, Angew. Chem. Int. Edit. 49 (2010) 3169–3172.
[39] A.J. Eskola, O. Welz, J. Zádor, I.O. Antonov, L. Sheps, J.D. Savee, D.L. Osborn, C.A. Taatjes, Probing the low-temperature chain-branching mechanism of n-butane autoignition chemistry via time-resolved measurements of ketohydroperoxide formation in photolytically initiated n-C_4H_{10} oxidation, Proc. Combust. Inst. 35 (2015) 291–298.
[40] K.A. Sahetchian, R. Rigny, S. Circan, Identification of the hydroperoxide formed by isomerization reactions during the oxidation of n-heptane in a reactor and CFR engine, Combust. Flame 85 (1991) 511–514.
[41] F. Battin-Leclerc, O. Herbinet, P.-A. Glaude, R. Fournet, Z. Zhou, L. Deng, H. Guo, M. Xie, F. Qi, New experimental evidences about the formation and consumption of ketohydroperoxides, Proc. Combust. Inst. 33 (2011) 325–331.
[42] K. Moshammer, A.W. Jasper, D.M. Popolan-Vaida, A. Lucassen, P. Diévart, H. Selim, A.J. Eskola, C.A. Taatjes, S.R. Leone, S.M. Sarathy, Y. Ju, P. Dagaut, K. Kohse-Höinghaus, N. Hansen, Detection and identification of the keto-hydroperoxide ($HOOCH_2OCHO$) and other intermediates during low-temperature oxidation of dimethyl ether, J. Phys. Chem. A 119 (2015) 7361–7374.
[43] E.J. Hamilton, S. Korcek, L.R. Mahoney, M. Zinbo, Kinetics and mechanism of the autoxidation of pentaerythrityl tetraheptanoate at 180–220 °C, Int. J. Chem. Kinet. 12 (1980) 577–603.
[44] R.K. Jensen, S. Korcek, L.R. Mahoney, M. Zinbo, Liquid-phase autoxidation of organic compounds at elevated temperatures. 1. The stirred flow reactor technique and analysis of primary products from n-hexadecane autoxidation at 120–180 °C, J. Am. Chem. Soc. 101 (1979) 7574–7584.
[45] R.K. Jensen, S. Korcek, L.R. Mahoney, M. Zinbo, Liquid-phase autoxidation of organic compounds at elevated temperatures. 2. Kinetics and mechanisms of the formation of cleavage products in n-hexadecane autoxidation, J. Am. Chem. Soc. 103 (1981) 1742–1749.
[46] R.K. Jensen, M. Zinbo, S. Korcek, HPLC determination of hydroperoxidic products formed in the autoxidation of n-hexadecane at elevated temperatures, J. Chromatogr. Sci. 21 (1983) 394–397.
[47] A. Jalan, I.M. Alecu, R. Meana-Pañeda, J. Aguilera-Iparraguirre, K.R. Yang, S.S. Merchant, D.G. Truhlar, W.H. Green, New pathways for formation of acids and carbonyl products in low-temperature oxidation: the korcek decomposition of γ-ketohydroperoxides, J. Am. Chem. Soc. 135 (2013) 11100–11114.
[48] E. Ranzi, C. Cavallotti, A. Cuoci, A. Frassoldati, M. Pelucchi, T. Faravelli, New reaction classes in the kinetic modeling of low temperature oxidation of n-alkanes, Combust. Flame 162 (2015) 1679–1691.
[49] W.J. Pitz, C.J. Mueller, Recent progress in the development of diesel surrogate fuels, Prog. Energy Combust. Sci. 37 (2011) 330–350.
[50] S.M. Sarathy, G. Kukkadapu, M. Mehl, W. Wang, T. Javed, S. Park, M.A. Oehlschlaeger, A. Farooq, W.J. Pitz, C.-J. Sung, Ignition of alkane-rich FACE gasoline fuels and their surrogate mixtures, Proc. Combust. Inst. 35 (2015) 249–257.
[51] F. Qi, Combustion chemistry probed by synchrotron VUV photoionization mass spectrometry, Proc. Combust. Inst. 34 (2013) 33–63.
[52] N. Hansen, T.A. Cool, P.R. Westmoreland, K. Kohse-Höinghaus, Recent contributions of flame-sampling molecular-beam mass spectrometry to a fundamental understanding of combustion chemistry, Prog. Energy Combust. Sci. 35 (2009) 168–191.
[53] J.A. Montgomery, M.J. Frisch, J.W. Ochterski, G.A. Petersson, A complete basis set model chemistry. VI. Use of density functional geometries and frequencies, J. Chem. Phys. 110 (1999) 2822–2827.
[54] R.B.M.J. Frisch et al., Gaussian 09, Gaussian, Inc., Wallingford, CT, 2009.
[55] S.M. Sarathy, T. Javed, F. Karsenty, A. Heufer, W. Wang, S. Park, A. Elwardany, A. Farooq, C.K. Westbrook, W.J. Pitz, M.A. Oehlschlaeger, G. Dayma, H.J. Curran, P. Dagaut, A comprehensive combustion chemistry study of 2,5-dimethylhexane, Combust. Flame 161 (2014) 1444–1459.
[56] J. Badra, A. Farooq, Site-specific reaction rate constant measurements for various secondary and tertiary H-abstraction by OH radicals, Combust. Flame 162 (2015) 2034–2044.
[57] R. Sivaramakrishnan, J.V. Michael, Rate constants for OH with selected large alkanes: shock-tube measurements and an improved group scheme, J. Phys. Chem. A 113 (2009) 5047–5060.
[58] G.E. Quelch, M.M. Gallo, M. Shen, Y. Xie, H.F. Schaefer, D. Moncrieff, Aspects of the reaction mechanism of ethane combustion. 2. Nature of the intramolecular hydrogen transfer, J. Am. Chem. Soc. 116 (1994) 4953–4962.
[59] J.D. DeSain, C.A. Taatjes, J.A. Miller, S.J. Klippenstein, D.K. Hahn, Infrared frequency-modulation probing of product formation in alkyl + O_2 reactions. Part IV. Reactions of propyl and butyl radicals with O_2, Faraday Discuss 119 (2002) 101–120.
[60] J.D. DeSain, S.J. Klippenstein, J.A. Miller, C.A. Taatjes, Measurements, theory, and modeling of OH formation in ethyl + O_2 and propyl + O_2 reactions, J. Phys. Chem. A 107 (2003) 4415–4427.
[61] S.M. Villano, L.K. Huynh, H.-H. Carstensen, A.M. Dean, High-pressure rate rules for alkyl + O_2 reactions. 1. The dissociation, concerted elimination, and isomerization channels of the alkyl peroxy radical, J. Phys. Chem. A 115 (2011) 13425–13442.
[62] J.D. Surratt, A.W.H. Chan, N.C. Eddingsaas, M. Chan, C.L. Loza, A.J. Kwan, S.P. Hersey, R.C. Flagan, P.O. Wennberg, J.H. Seinfeld, Reactive intermediates revealed in secondary organic aerosol formation from isoprene, Proc. Natl. Acad. Sci. USA 107 (2010) 6640–6645.
[63] N.C. Cole-Filipiak, A.E. O'Connor, M.J. Elrod, Kinetics of the hydrolysis of atmospherically relevant isoprene-derived hydroxy epoxides, Environ. Sci. Technol. 44 (2010) 6718–6723.
[64] S. Sharma, S. Raman, W.H. Green, Intramolecular hydrogen migration in alkylperoxy and hydroperoxyalkylperoxy radicals: accurate treatment of hindered rotors, J. Phys. Chem. A 114 (2010) 5689–5701.

[65] T.F. Mentel, M. Springer, M. Ehn, E. Kleist, I. Pullinen, T. Kurtén, M. Rissanen, A. Wahner, J. Wildt, Formation of highly oxidized multifunctional compounds: autoxidation of peroxy radicals formed in the ozonolysis of alkenes—deduced from structure–product relationships, Atmos. Chem. Phys. 15 (2015) 6745–6765.
[66] S. Solomon, D. Qin, M. Manning, Z. Chen, M. Marquis, K.B. Averyt, M. Tignor, H.L. Miller (Eds.), Climate Change 2007: The Physical Science Basis, Cambridge University Press, Cambridge, United Kingdom/New York, NY, USA, 2007 p. 996.
[67] N. Blin-Simiand, F. Jorand, K. Sahetchian, M. Brun, L. Kerhoas, C. Malosse, J. Einhorn, Hydroperoxides with zero, one, two or more carbonyl groups formed during the oxidation of n-dodecane, Combust. Flame 126 (2001) 1524–1532.
[68] A. Miyoshi, Systematic computational study on the unimolecular reactions of alkylperoxy (RO_2), hydroperoxyalkyl (QOOH), and hydroperoxyalkylperoxy (O_2QOOH) radicals, J. Phys. Chem. A 115 (2011) 3301–3325.
[69] J. Bugler, K.P. Somers, E.J. Silke, H.J. Curran, Revisiting the kinetics and thermodynamics of the low-temperature oxidation pathways of alkanes: a case study of the three pentane isomers, J. Phys. Chem. A 119 (2015) 7510–7527.
[70] S.M. Villano, L.K. Huynh, H.-H. Carstensen, A.M. Dean, High-pressure rate rules for alkyl + O_2 reactions. 2. The isomerization, cyclic ether formation, and β-scission reactions of hydroperoxy alkyl radicals, J. Phys. Chem. A 116 (2012) 5068–5089.
[71] M. Pelucchi, M. Bissoli, C. Cavallotti, A. Cuoci, T. Faravelli, A. Frassoldati, E. Ranzi, A. Stagni, Improved kinetic model of the low-temperature oxidation of n-heptane, Energy Fuels 28 (2014) 7178–7193.